OPEN ACCESS RESEARCH ARTICLE

Fire-resistivity personification of waterborne intumescent flame-retardant nano-coatings for steel structures: Synthesis and Characterization

A. Nour El-Dein[a,]*, Emad M. Gad[b] , Ashraf M. El-saeed[c], Ossama M. Abo-elenien[c]

a-Egyptian Natural Gas Company (GASCO).
b-Suez Canal University, Faculty of science.
c- Egyptian Petroleum Research Institute (EPRI), Nasr City 11727, Cairo, Egypt.
** Corresponding author: A. Nour El-Dein[a]*

ABSTRACT
This research is aimed to the preparation of Phenol-formaldehyde Bentonite Nanocomposite (PFBN) containing a variety of functional groups utilizing one step acid-catalyzed addition-condensation of phenol, formaldehyde and H-bentonite; direct synthesis of monophasic ultrafine pure particles of Cobalt Ferrite Nano-LDH (layered double hydroxide) (C_{Fn2}) and the synthesizing of Nano Zinc Borate (C_{Fn1}) by coordination homogeneous precipitation method. Materials were prepared, purified and morphologically confirmed by fourier transform infrared (FTIR), proton nuclear magnetic resonance (^{1}HNMR), energy-dispersive X-ray microanalysis (EDXA), X-Ray diffraction (XRD) and high-resolution transmission electron microscopy (HRTEM). The planed strategy in our nearly future research is the utilizing of the synthesized materials as waterborne intumescent flame-retardant nano-coatings for steel structures; PFBN have been chosen as a binder, carbon source and a potential flame-retardant; C_{Fn2} and C_{Fn1} were selected as a possibly anticorrosive and fire retardant additives .

Keywords: Phenol-formaldehyde, Bentonite, Borate and LDH compounds; FTIR; ^{1}HNMR, EDXA, XRD and HRTEM

Date of Submission: 08 -08-2017 Date of acceptance: 19-08-2017

I. INTRODUCTION

Nanoscience is at present empowering transformative changes in a few innovation zones yet new ideal models will in the end have a considerably more extensive and progressive effect. In the territory of coatings, new methodologies using nanoscale impacts can be utilized to make coatings with essentially improved or upgraded properties.[1] Nano-composites have gotten much enthusiasm over the previous decades because of their critical focal points over traditional composites, in which high loadings of added substances are frequently required.[2-9] The definition of nano-composite material has over the years broadened significantly to encompass a large variety of systems such as one-dimensional, two-dimensional, three-dimensional and amorphous materials, made of distinctly dissimilar components and mixed at the nanometer scale. Nano-composites are "materials with a nanoscale structure that improve the macroscopic properties of products."[10] the typically, nano-composites are clay, carbon, or polymer, or a combination of these materials with nanoparticle building blocks. Nano-composite can be defined also as a multiphase solid material where one of the phases has one, two or three dimensions of less than 100 nanometers (nm), or structures having nano-scale repeat distances between the different phases that make up the material.[11] The mechanical, electrical, thermal, optical, electrochemical, catalytic properties of the nano-composite will differ markedly from that of the component materials. Layered double hydroxides (LDHs), also known as anionic clays, are a family of compounds which are deserving much attention in recent years.[12-14] Synthetic layered double hydroxide (LDH) mixes are vital modern materials utilized as sponges, polymer stabilizers, antacid impetuses, corrosive killing operators, and antecedents in the arrangement of spinel ceramics.[15,16]

LDH mixes comprise of emphatically charged layers of blended metal hydroxides isolated by adversely charged layers of anions and water.[17,18]

LDH are structurally similar to brucite, $Mg(OH)_2$, with one notable difference: LDH are mixed-metal hydroxides and brucite is a magnesium hydroxide. The most commonly studied LDH consists of divalent and trivalent metals (M), with the general formula:[19-22]

$$[\ M^{(II)}_{1-X}\, M^{(III)}_{x}\, (OH)_2\ ]^{+}\, [A^{n-}]_{x/n}\ .\ yH_2O$$

The values of x vary,[23,24] but typically fall within the range: $0.25 \leq x \leq 0.33$, such that the above formula corresponds to a range from $[\ M^{(II)}_{0.75}\, M^{(III)}_{0.25}\, (OH)_2\ ]\ [\ A^{n-}\ ]_{x/n}\ .\ yH_2O$ to $[\ M^{(II)}_{0.67}\, M^{(III)}_{0.33}\, (OH)_2\ ]\ [\ A^{n-}\ ]_{x/n}\ .\ yH_2O$.

In whole number proportions, these two formulas transform into $[M^{(II)}_2M^{(III)}(OH)_6][A^{n-}]_{x/n}.yH_2O$ and $[M^{(II)}_3M^{(III)}(OH)_6][A^{n-}]_{x/n}.yH_2O$, which are simplified as either a 2:1 LDH or a 3:1 LDH, respectively. The values for y are dependent on the anion and conditions, with two being the most common.

Fire retardants (FR) are chemicals utilized as a part of thermoplastics, thermo sets, materials and coatings that hinder or oppose the spread of flame.

To make a polymer fire safe, intumescent fire resistant's (IFRs) must be included at moderately high stacking (15 % to 25 % by mass) to effectively breeze through flame tests, and subsequently, the polymer composites produced endure huge misfortunes in mechanical quality and liquefy viscosity.[25]

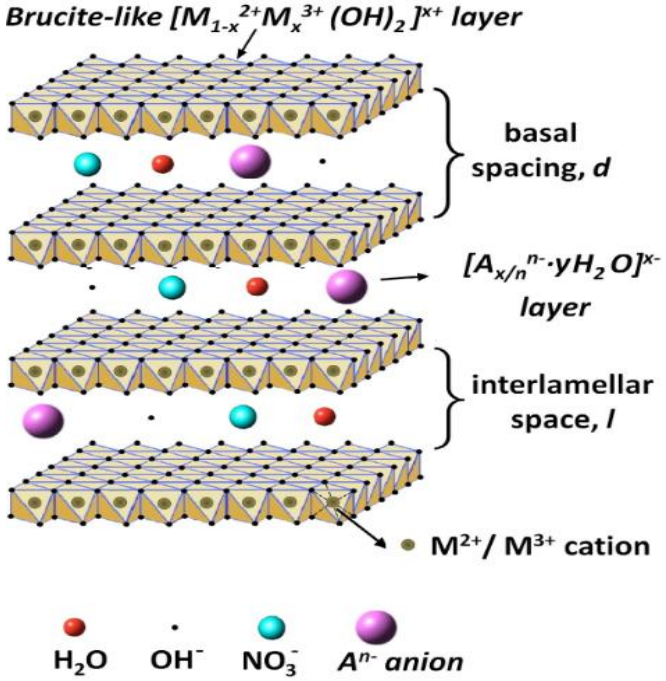

Scheme 1 Schematic illustration of General crystal structure of LDH compounds.

The use of fire retardant coatings is one of the easiest, one of the oldest and one of the most efficient ways to protect materials against fire.[26,27] Indeed, it presents several advantages: it does not modify the intrinsic properties of the materials (e.g. the mechanical properties), it is easily processed and may be used onto several materials such as metallic materials,[28] polymers,[29] textiles[30] and wood.[31] Moreover, since ignition occurs usually on the surface of a material it is important to concentrate the protective action at this place. The objective of this study is to prepare nano-composite of phenol-formaldehyde bentonite **(PFBN)** having various functional groups by one step acid-catalyzed addition-condensation of phenol, formaldehyde and H-bentonite. The synthesizing of crystalline, monophasic, ultrafine and pure particles of cobalt ferrite nano-LDH ($\mathbf{C_{Fn2}}$) using Fe and Co nitrates. Preparation of zinc borate nanoparticles ($\mathbf{C_{Fn1}}$) utilizing coordination homogeneous precipitation method.

II. EXPERIMENTAL

2.1. Chemicals and materials

All chemicals utilized as parts of this article were accessible and utilized as-received without extra purging. Phenol, Formaldehyde, $Co(NO_3)_2.6H_2O$, $Fe(NO_3)_3.9H_2O$, Na NO_3, ZnO and H_3BO_3 were obtained from sigma Aldrich. Ammonia (25 wt.%) and commercial bentonite clay (obtained from the egyptian chemical stores) were also used. The deionized water was utilized for setting up the sample solutions.

2.2. Preparation

2.2.1 Preparation of Cobalt Ferrite Nano- LDH (C_{Fn2})

In the direct synthesis of Cobalt Ferrite Nano-LDH $[Co_{0.67}Fe_{0.33}(OH)_2]$ $(NO_3)_{0.33}.2H_2O$, (0.050 mol) of $Co(NO_3)_2.6H_2O$ and (0.025 mol) of $Fe(NO_3)_3.9H_2O$ were dissolved in 100 ml of deionized water. This solution was then added drop wise to 200 ml of (0.25 mol) $NaNO_3$ solution at pH10 and vigorous stirring. The pH10 of the slurry was held constant at 10 ± 0.3 during the synthesis by the addition of 2 M NaOH solution, as needed. The addition was over 90 min and the reaction mixture was kept at 298 ± 1 K. To exclude the CO_2 presence, N_2 gas was preliminarily purged through all solutions for 1 hr, and continued bubbling through the slurry during the synthesis. Carbonate-free water obtained by vigorously boiling deionized water for 15 minutes prior to use was used for the solution preparation. The formation of a white precipitate was observed during the synthesis. Nitrate was chosen as the gegen ion due to the relative ease with which the nitrate anions can be displaced from the interlayer. The resultant slurry was kept at 338 K for 24 hr in a closed N_2-purged vessel for crystallization of the LDH particles and then was centrifugated and washed four times with carbonate-free deionized water until pH = 7 was reached. To diminish the mean size of LDH particles, the gel obtained after final centrifugation was ultrasonically treated for 30 min after addition of a small amount of deionized water. Finally the washed precipitate was dried at 333 K during 24 hr in a vacuum oven.

2.2.2 Preparation of Nano Zinc Borate (C_{Fn1})

Firstly, a complex solution was formed by adding (0.05 mol) of ZnO into 100.0 mL of (1.5 mol dm^{-3}) H_3BO_3 solution and 25 ml concentrated ammonia (25 wt.%) under vigorous stirring at room temperature, the complex solution was added into 150.0 mL distilled water secondly, then the reaction was carried out using magnetic stirring at 318 K for 4 hr. Finally, a large amount of white sediment was formed. The precipitate was separated by centrifuge and rinsed with distilled water to remove the adsorbed ions, then dried in a vacuum oven at 343 K for 12 hr.

The mechanism of the coordination homogeneous precipitation strategy is as per the following: right off the bat, zinc particles respond with ammonia, framing an intricate arrangement existing together with precipitator boric acid. Along these lines the complex separates to discharge the metal particles by means of weakening the mind boggling arrangement with water and warming the perplexing answer for expel ammonia from aqueous solution. At the point when the zinc particles achieve a specific sum, the zinc borate residues are shaped in the arrangement. Since the metal particles and the precipitator are scattered in the arrangement homogeneously, therefore the precipitation response of metal particles and precipitator can achieve molecular level, which guarantees the sedimentation of fancied nanomaterials yielding and isolating out homogeneously from the arrangement.

2.2.3 Preparation of Nano-composite

2.2.3.1 Bentonite clay purification

Sample dispersion: The Bentonite clay was suspended in deionized water for 24 hr while stirring using a magnetic stir-bar and plate to hydrate the clay. The suspension was obtained by mixing 5.0 g of clay with 100 mL of deionized water in a 250 mL centrifuge bottle.

Particle-size fractionation: To obtain the < 2 μm clay-sized particles the clay suspension was centrifuged for 6 min at (~600 rpm). The supernatant liquid suspension containing the < 2 μm clay-sized particles was siphoned into a 250 mL centrifuge bottle. The pellet containing the > 2 μm particles was re-suspended with 100 mL of deionized water by mixing briefly, and then subjected to low-speed centrifugation as before to recover additional clay-sized particles. The supernatant suspension was siphoned and added to the previously collected suspension of clay sized materials.

Chemical removal of carbonate: The suspension of clay-sized particles from above was titrated with 0.5 M Na acetate buffer (pH 5.0) until a pH of 6.8 was obtained; the sample was stirred for one more hour during which the pH remained stable. This step was repeated three times until the pH remained constant at 6.8 for 30 min.

Removal of soluble salts: To promote flocculation of the clay, ~1.5 g NaCl were added to the bottle containing the clay suspension and stirred for ~5 min until the salt was dissolved, then the suspension was centrifuged for 20 min at (4500 rpm). The supernatant liquid was discarded, and the clay pellet re-suspended in 200 mL of deionized water by laying the centrifuge bottle on a rotary shaker and shaking at 120 rpm for 8 h. The clay suspension was again centrifuged at (4500 rpm) for 30 min and the supernatant liquid discarded. The precipitate was then dried in a vacuum oven at 343 K for 12 hr.

2.2.3.2 Bentonite clay acidification

10 g of bentonite were added to 500 ml of 1 N HCl in a 1 L three-necked flask, and stirred vigorously for 12 hr at 353 K. The clay was filtered and washed with distilled water repeatedly up to pH7 until no chloride was detected with a drop of 0.1M $AgNO_3$ solutions. Then the ion-exchanged clay (H-Bentonite) was air-dried for several days, and ground to pass a 300-mesh sieve.

2.2.3.3 **Preparation of Phenol-Formaldehyde Bentonite Nano-composite (PFBN)**

10 gm of H-Bentonite was mixed with phenol, formaldehyde (P/F molar ratio 1: 0.85) in a 250 ml three-necked flask, and stirred vigorously at room temperature for 1 hr. The mixture was heated to 368 K at a heating rate of 5 K/min, and reaction was continued at that temperature up to the complete consumption of formaldehyde. The product was then dehydrated in vacuum in a rotatory evaporator at about 353 K to obtain the phenol-formaldehyde bentonite nano-composite. The product was obtained and purified by vacuum distillation.

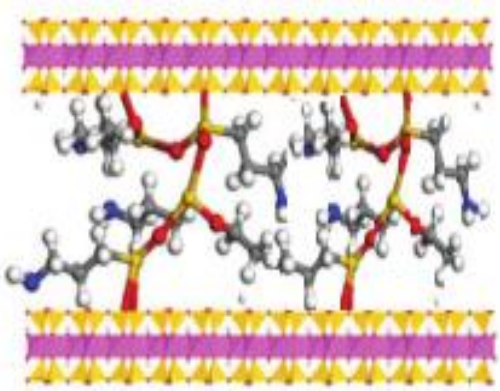

Scheme 2 Schematic Illustration of Phenol-Formaldehyde Bentonite Nano-composite (PFBN).

2.3 Characterization methods

The morphologies analyses of LDH, Nano-Borate and Nano-composites were taken on:

Fourier transform infrared (FTIR) spectra were obtained using the KBr method on a mattson – infinity series bench top 961 spectrometer operated at 1 cm^{-1} resolution in the 400–4000 cm^{-1} region.

Proton Nuclear magnetic resonance (^{1}HNMR) spectra were obtained using 300 MHZ spectrometer W-P-300, Bruker. The solution for ^{1}HNMR analysis was prepared by dissolving the prepared compounds in dimethyl sulphoxide (DMSO).

Energy-dispersive X-ray microanalysis (EDXA) spectra were obtained using JEOL JEM-2100 Transmission Electron Microscope (TEM) combined with Energy dispersive spectrometer (EDXA) operated at 200 kV.

X-Ray Diffraction (XRD) spectra were obtained using a Philips PW3710 X-ray diffractometer for the composites. CuKα (λ = 1.54Å) radiation, generated at a voltage of 40 kV and current of 55mA was used as the X-Ray source. The diffraction patterns were collected at a diffraction angle 2θ from 1^o to 100^o at a scanning rate and step size of 3^o/min and 0.1^o, respectively.

High-resolution Transmission Electron Microscopy (HRTEM) Electron micrographs of the samples were taken by using JEOL JEM-2100 Transmission Electron Microscope operated at an acceleration voltage of 200 kV.

III. RESULTS AND DISCUSSION

3.1 Morphological Analysis

In order to elucidate the prepared materials, their characterizations were carried out by determining their spectroscopic and morphology.

3.1.1 FTIR Interpretation

The structure of arranged materials can be promptly controlled by measuring their infrared spectra utilizing a Fourier transform infrared (FTIR) spectrometer and afterward contrasting the outcomes and the accessible ghostly information base. In the elucidation of the prepared compounds, the evidence for the preparation originates from the FTIR studies.

Figure 1 illustrates the FTIR spectrum of the prepared **(PFBN)** nano-composite. The characteristic band observed at 470, 536 and 818 cm^{-1} wavelength indicates out-of-plane bending vibration of aromatic C–H: C–H bend. The peaks at around 691 cm^{-1} are assigned to stretching vibration of Si–O deformation parallel to the optical axis. The 755 cm^{-1} band corresponds to out-of-plane aromatic ring deformation by 1, 2, and 4 links. The peaks at around 913 cm^{-1} are assigned to stretching vibration of Si–O deformation perpendicular to the optical axis. The 1035 cm^{-1} band have been specifically assigned to deformation of OH group attached to Al^{+3} and Mg^{+2}. The 1101 cm^{-1} band have been specifically assigned to deformation of OH group attached to Al^{+3} and Fe^{+3}. The 1165 cm^{-1} band have been specifically assigned to deformation of OH group attached to $2Al^{+3}$.The presence of the band at 1231 cm^{-1} is characteristic of the Si-O-Si linkage in which assigned to asymmetric stretching vibrations. The peak at around 1361 cm^{-1} represents in plane stretching vibration of Si–O. In addition, the 1453 cm^{-1} peak indicates Methylene Bridge, which is typical of Phenol-Formaldehyde. The peak observed at 1509 cm^{-1} wavelength indicates H–O–H deformation. The band appeared at 1595 cm^{-1} for stretching vibration of Aromatic –C–C– in ring ArC-C stretch. The band appeared at 3019 cm^{-1} for Aromatic stretching vibration of C—H Ar–H stretch. The band at 3649 cm^{-1} is due to the phenolic O—H stretch. The band observed at 3696 cm^{-1} for stretching vibration of O—H (Mg, Al)—OH stretch.

Figure 1 illustrates the FTIR spectrum of the prepared **Cobalt Ferrite** Nano-LDH (C_{Fn2}). The characteristic vibration broad band absorption peak at 3345 cm^{-1} is du to O–H asymmetric and symmetric stretching vibration modes in the brucite-like layers and the interlamellar water molecules, while the broadening of the band is assigned to formation of

hydrogen bond.[32] Bending vibrations of H-O-H band of the interlayer water molecules is indicated with the band at 1630 cm^{-1}.[33,34] The sharp absorption peaks of the nitrate anion at 1430 cm^{-1} are intense in the spectrum which attributed to the ν_3 (asymmetric N–O stretch) stretching vibration of the NO_3^- groups in the LDH interlayer. A weak band located at 795, 939 and 1136 cm^{-1} wavelength, arises from the stretching modes ν_4 (in-plane bending mode), ν_2 (out-of plane deformation mode) and $2\nu_2$ (out-of plane deformation mode overtone) respectively, which confirm the presence of nitrate group, the intergallery NO_3^- anion possesses D_{3h} symmetry in the Co/Fe LDH interlayer. The absorption band of Co↔O and Fe↔O bonds appeared at 553 cm^{-1}.[35]

Figure 1 illustrates the FTIR spectrum of the prepared **Nano Zinc Borate** (C_{Fn1}). The FTIR spectra ascribes that the band which indicates stretching vibrations of O-H was obvious at 3459 cm^{-1}.[36] Bending vibrations of H-O-H band which were due to crystal water included in compound was slightly seen at 1647 cm^{-1}.[36] The presence of the band at 1341 cm^{-1} assigned to asymmetric stretching vibrations of trihedral (BO_3) borate groups.[37] The peaks at around 1060 and 928 cm^{-1} were assigned to asymmetric and symmetric stretching vibrations of tetrahedral (BO_4) borate groups.[37] The peak observed at 675 cm^{-1} wavelength indicated in plane bending vibrations of trihedral (BO_3) groups.[38]

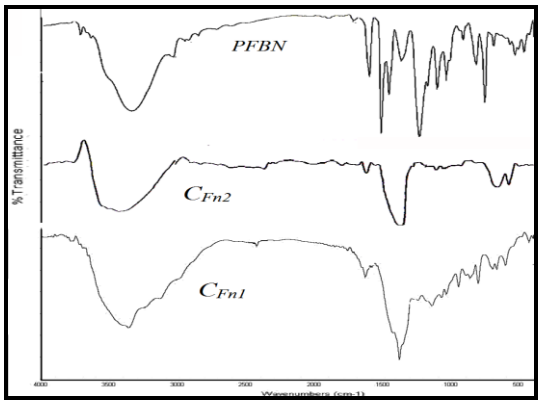

Figure 1 FTIR spectra of PFBN, C_{Fn2} and C_{Fn1}

3.1.2 ^{1}HNMR Interpretation

A representative ^{1}HNMR spectrum of nano-composite **PFBN** is shown in Figure 2. ^{1}HNMR Figure 2 showed that each peak was assignable to the corresponding proton. Inspection of Figures reveal that the splitting pentlet signal at chemical shift δ = 2.5 ppm is from the solvent DMSO (dimethylsulfoxide) and is disregarded. In particular, we focused on the chemical shift around δ =3.3, 3.96 ppm of the ortho–ortho, ortho–para and para–para methylene bridge linkages. The chemical shift around δ = 4.6 ppm was originated from the aromatic hydroxyl proton HO-Ar. The chemical shift around δ = 5.4 ppm for the proton of C=C-H. The chemical shift splitting high order signal around δ = 6.7 ppm was originated from the aromatic proton Ar-H.

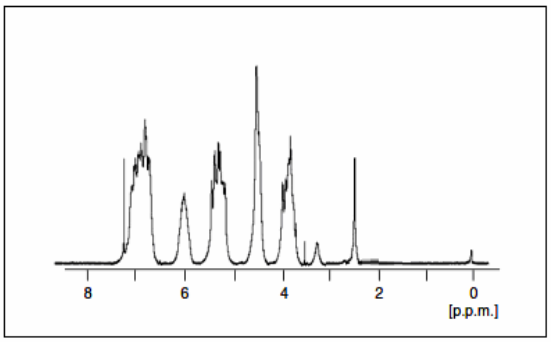

Figure 2 ^{1}HNMR spectra of (PFBN)

3.1.3 Energy-dispersive X-ray microanalysis (EDXA) interpretation

Element analysis of **Cobalt Ferrite** Nano-LDH (**C_{Fn2}**) LDH by EDXA demonstrated that for the most part three components (O, Co and Fe) existed in the Nano-LDH (C_{Fn2}) Figure 3, what's more, the Co/Fe mole proportion was kept at 2:1.

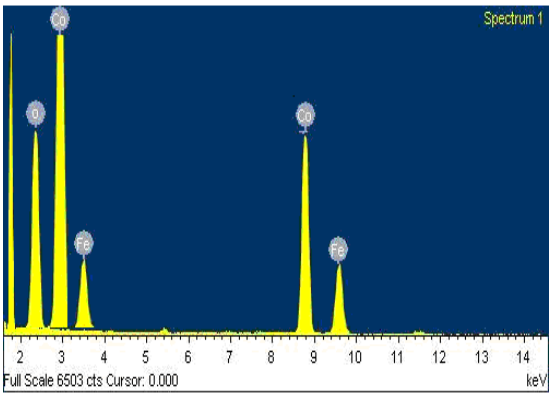

Figure 3 EDXA spectra of (C_{Fn2})

EDXA spectra of the prepared (C_{Fn1}) Nano-Borate shown in Figure 4 confirms that the Nano-Borate consist of zinc, boron and oxygen elements with the desired stoichiometric of $ZnO{\cdot}3B_2O_3$. Table 1 showed element analysis of (C_{Fn1}) by EDXA.

Table 1 Element analysis of C_{Fn1} by EDXA (Atomic %)

Compound	C_{fn1}
Formula weight	497.78
Empirical Formula	$2ZnO{\cdot}3B_2O_3{\cdot}7H_2O$
Zn%	26.25
B%	13.05
O%	57.89

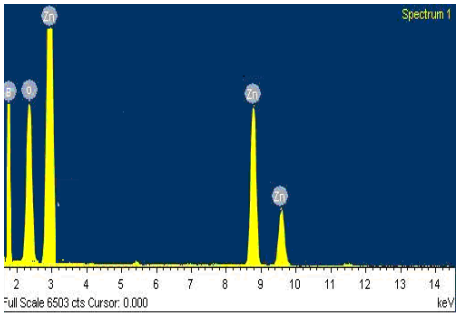

Figure 4 EDXA spectra of (C_{Fn1})

3.1.4 X-Ray Diffraction (XRD) spectra interpretation

X-Ray Diffraction (XRD) pattern for the [Co–Fe–NO3] Figure 5 show that the sample, which consists of a single phase, is very well crystallized with its constituting crystallites of large size. XRD is performed on (C_{Fn2}) to gain statistically relevant information about their crystallographic structure. The diffracting planes that were characteristic of an LDH structure were clearly observed.[39] The basal diffracting planes are (003), (006), (012), (110), and (113). The (003) basal diffracting plane spacing was determined to be 7.64 A˚.[39,40] The peak corresponding to the (110) diffracting plane was very distinct, signifying a regular arrangement of the metal ions in the Co–Fe LDH.[41,42] Meanwhile, more non-basal diffracting plane, (101) had been observed. This meant that (C_{Fn2}) had higher crystallinities, including non-basal diffracting plane. This pattern is in agreement with that found for crystallites using HRTEM technique Figure 9. The XRD powder data, refined on the hexagonal setting with a rhombohedral symmetry (space group: Hexagonal scalenohedral rhombohedral holohedral (R3m), provided the lattice parameters for the sample: the cell parameter a, which is related to metal–metal interatomic distance within the sheets, a = 0.380nm, and the cell parameter c, which is a measure of the interlayer distance d, with c = 3d, c = 2.292nm. The interlayer distance, d = 0.764nm.

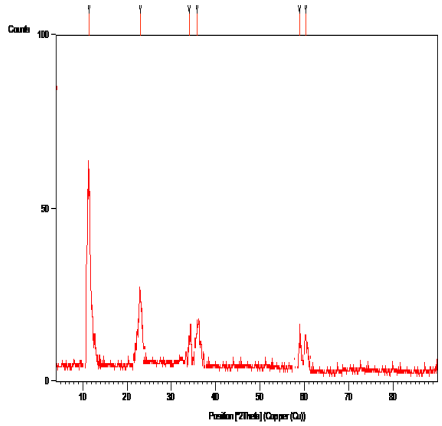

Figure 5 XRD pattern of LDH (C_{Fn2})

Figure 6 shows an X-Ray Diffraction (XRD) pattern for the Nano Zinc Borate (**C_{Fn1}**), from which the sample, which consists of a single phase, is well crystallized with its constituting crystallites. XRD is performed on (C_{Fn1}) to gain statistically relevant information about their crystallographic structure. The diffracting planes which characteristic of the prepared structure were clearly observed.[43-46] The basal diffracting planes are (003), (006), (009) and (012). The (006) basal diffracting plane spacing was determined to be 4.05 A˚. This pattern is in agreement with that found for crystallites using HRTEM technique Figure 11. The peak positions and the relative intensities of the peaks indicated that the sample had main reflections at 2 theta values of 21.9700 for reflections of (006) plane. In the X-ray diagrams of the precipitates obtained in the present study, the size of the crystals perpendicular to (006) plane were in the mean size of crystal of 5.86 nm as determined from the breadth of the related diffraction peak and by Scherrer Equation (Equation 1). The XRD powder data, refined on the setting with a rhombohedral symmetry (space group: scalenohedral rhombohedral holohedral (R3m), provided the lattice parameters for the sample: the cell parameter a, which is related to metal–metal interatomic distance within the sheets, a = 0.287 nm, and the cell parameter c, which is a measure of the interlayer distance d, with c = 3d, c = 1.215nm. The interlayer spacing, d = 0.405nm.

$$\tau = K \lambda / \beta_s(2\theta)_{hkl} \cos\theta_{hkl} \qquad (1)$$

Where:

- **τ** is the mean size of the ordered (crystalline) domains, which may be smaller or equal to the grain size (the average thickness of the crystal in a direction normal to the diffracting plane hkl);
- **K** is (a constant near unity) a dimensionless shape factor.
- **λ** is the wavelength of incident X-ray beam ($1.5406A^o$);
- $\boldsymbol{\beta_s(2\theta)_{hkl}}$ is (the crystallite size contribution to the peak width (integral or full width at half maximum) in radians) the line broadening at half the maximum intensity (FWHM), after subtracting the instrumental line broadening, in radians. This quantity is also sometimes denoted as Δ(2θ);

$\boldsymbol{\theta_{hkl}}$ is the Bragg diffraction angle (in degrees).

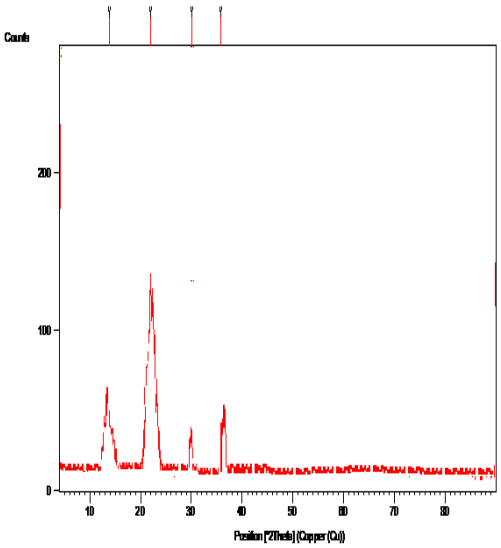

Figure 6 XRD pattern of LDH (C_{Fn1})

3.1.5 HRTEM micrograph interpretation

The HRTEM micrograph of the PFBN Nano-composite, shown in Figure 7, reveals the presence of single clay layers homogenously dispersed in the polymer matrix; the bright region represents the matrix portion, and the dark lines represent the clay nanolayer, which indicates the formation of a fully exfoliated Nano-composite. Interlayer clay distances turning out to vary from 5.35 nm to 9.95 nm.

This is in reverse with the typical clay structure, characterized by the presence of regular stacking arrangements, made by parallel layers. The enlarged spacing of Interlayer clay distances indicates the successful intercalation of polymer matrix to the layers of clay, thus making clay organophilic and facilitating the intercalation and dispersion of the polymer which is an organic material.

HRTEM analysis suggests that actually two factors play a significant role in nano-composite: the degree of intercalation (defined by the inter-laminar spacing, as revealed by XRD analysis), and the degree of dispersion (defined by the average number of lamellae in each stacking), which cannot be determined by XRD analysis. In order to better assess the Nano-composite crystallographic structure Selected Area Electron Diffraction patterns (SAED) of the sample have been analyzed (Figure 8). The SAED pattern exhibits highly dispersive diffraction sharp ring-spot pattern, indicating the formation of exfoliated, nanosized polymer matrix.

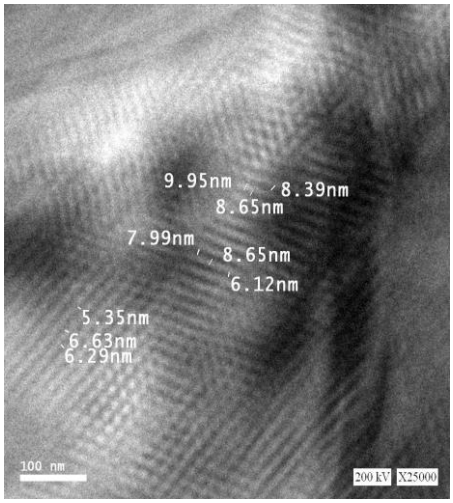

Figure 7 HRTEM spectra of (PFBN)

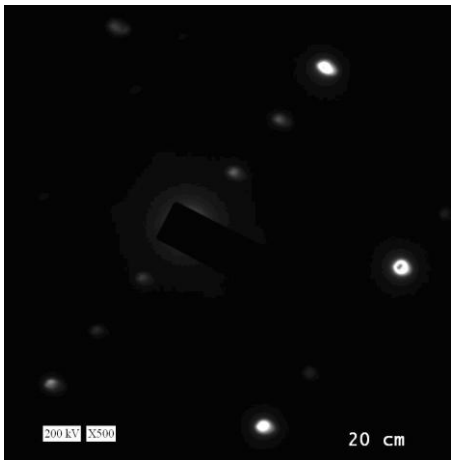

Figure 8 Electron diffraction pattern of neat compound (PFBN)

The HRTEM micrograph and particle size distributions of cobalt ferrite (C_{Fn2}) are shown in Figure 9. HRTEM micrograph was taken at the highest magnification of the system with the scale bar

of 20 nm in length as shown. The results indicate that the sample is uniform in both morphology and particle size distribution and reveals the occurrence of intercalated tactoids of LDH crystallites. The tactoids are mostly in the form of thin platelets having thickness in the range 0.6-1.0 nm and lateral dimension ranging from few nm about (5–10 nm), which is in good agreement with the XRD results. Images obtained for the LDH show evident hexagonal morphology and prevalence of ultrathin layer. The thickness of ultrathin LDH layers is deemed to be a molecular thickness, representing a positively charged host metallic layer with O–H bonded on the surface. The surfaces of all ultrathin LDH layers are having relatively smooth features.

The SAED pattern in Figure 10 exhibits polycrystalline diffraction rings consistent with 003, 006, 012, 015, 110 and 113 reflections. The 003 ring can be taken as an evidence of the hexagonal unit cell. The diffraction pattern is evidence of the strong superlattice reflections related to the hexagonal unit cell. No more sharp ring-spot patterns have appeared in the electron diffraction pattern, indicating the formation of fine, nanosized compound.

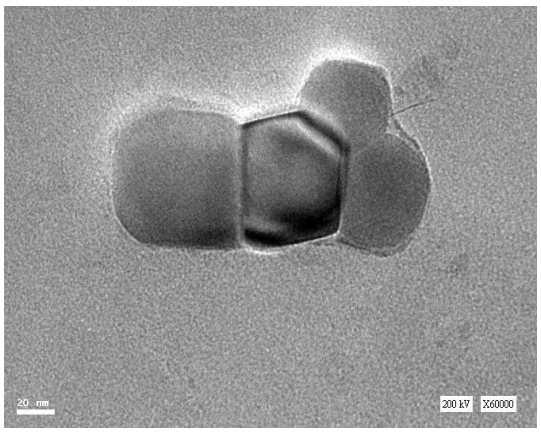

Figure 9 HRTEM image of (C_{Fn2})

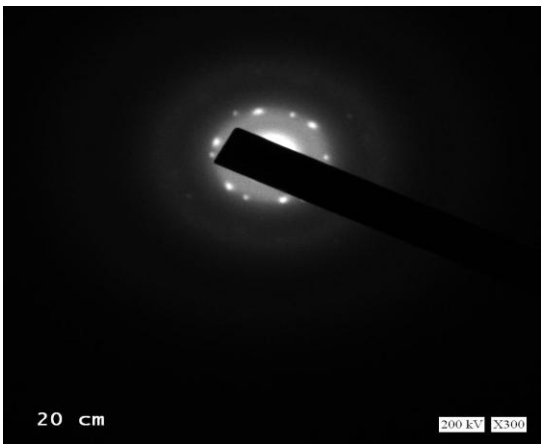

Figure 10 Electron diffraction pattern of neat compound (C_{Fn2})

Figure 11 shows the HRTEM microphotograph of the Zinc borate nanoparticles (C_{Fn1}). HRTEM micrograph was taken at the highest magnification of the system with the scale bar of 50 nm in length as shown. The particles have a regular bundle-like structure. Which indicate the zinc borate particles are uniform in both morphology and particle size distribution. A lattice fringes observed from the HRTEM image, which corresponds to lattice plane of monoclinic phase. The calculated particle size from the TEM is ranging from few nm about (2.35–5.65 nm), which is in good agreement with the XRD measurement.

In order to examine the crystallographic structure of prepared sample selected area electron diffraction (SAED) patterns was taken, which is shown in Figure 12. The SAED pattern exhibits polycrystalline diffraction rings consistent with 003, 006, 101, and 012 reflections. The diffracting planes are indexed as (202) and (402) reflections which are corresponding to the monoclinic phase of zinc borate, which is also observed from the X-ray diffraction pattern. No more sharp ring-spot patterns have appeared in the electron diffraction pattern, indicating the formation of fine, nanosized compound.

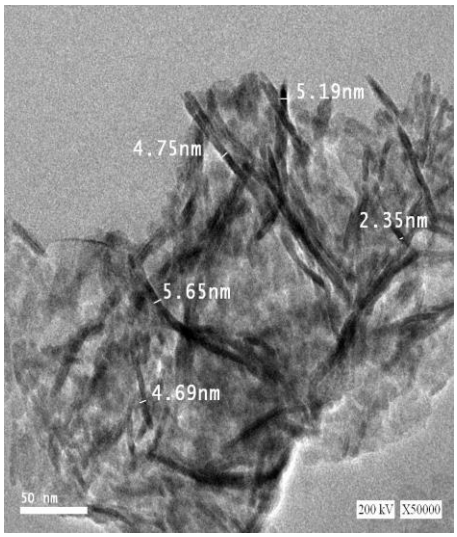

Figure 11 HRTEM image of (C_{Fn1})

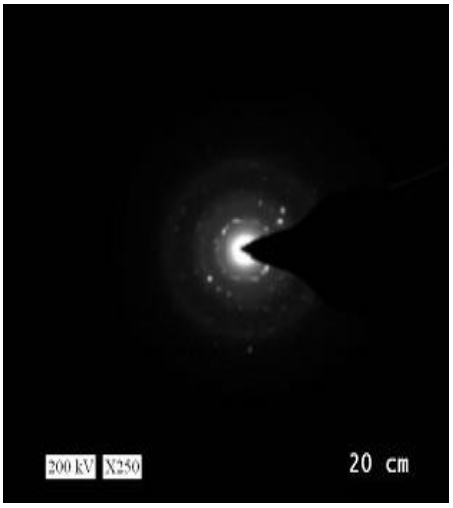

Figure 12 Electron diffraction pattern of neat compound (C_{Fn1})

IV. CONCLUSION

We successfully prepared nano-composite of phenol-formaldehyde bentonite **(PFBN)** having various functional groups by one step acid-catalyzed addition-condensation of designed phenol with formaldehyde and H-Bentonite. The effectively intercalation of Bentonite clay into Phenol-formaldehyde polymer matrix, and portrayed the built Nano-composite. In addition, HRTEM micrograph of PFBN nano-composite, uncovers the nearness of single clay layers homogenously scattered in the polymer network; the brilliant area speaks to the matrix partition, and the dim lines speak to the clay nanolayer, which demonstrates the arrangement of a completely exfoliated nano-composite.

The results demonstrates the possibility of synthesizing crystalline, monophasic, ultrafine and pure particles of cobalt ferrite Nano-LDH ($\mathbf{C_{Fn2}}$) using Fe and Co nitrates as precursors. Particles with sizes of 5.0 to 10.0 nm were obtained, as confirmed by TEM and XRD analyses. EDXA Element analysis demonstrated that mainly three elements (O, Co and Fe) existed in the Nano-LDH (C_{Fn2}), and the Co/Fe mole ratio was kept at 2:1. HRTEM micrograph obtained for the LDH demonstrates obvious hexagonal morphology and predominance of ultrathin layer.

Zinc Borate ($\mathbf{C_{Fn1}}$) nanoparticles was synthesized using the mechanism of the coordination homogeneous precipitation method. In this paper, by controlling the reaction conditions, we have successfully synthesized $2ZnO{\cdot}3B_2O_3{\cdot}7H_2O$ nanostructures morphologies, using ZnO, H_3BO_3 and ammonia as the reactants. Powder X-ray diffraction patterns confirmed a single phase well crystallized crystallites. The FT-IR spectrum clearly demonstrates the bands of metal ions and oxygen, asymmetric stretching vibrations of trihedral (BO_3) borate and tetrahedral (BO_4) borate groups groups.

REFERENCES

[1]. R. B. Donald, E. B. Paul, A. E. Anter, Progress in Organic Coatings, 47, (2003), 342-356.
[2]. J.W. Gilman, Appl. Clay Sci., 15, (1999), 31-49 .
[3]. J. Zhu, C.A. Wilkie, Polym. Int., 49, (2000), 1158-1163.
[4]. X. Fu, S. Qutubuddin, Polymer, 42, (2001), 807-813 .
[5]. J. Zhu, P. Start, K.A. Mauritz, C.A. Wilkie, Polym. Degrad. Stab., 77, (2002), 253-258.
[6]. P. Meneghetti, S. Qutubuddin, Thermochim. Acta, 442, (2006), 74-77.
[7]. T.Y.A. Fahmy, F. Mobarak, Carbohyd. Polym., 72, (2008), 751-755.
[8]. L.Y. Li, C.Y. Li, C.Y. Ni, L.X. Rong, B. Hsiao, Polymer, 48, (2007), 3452-3460.
[9]. S.H. Lee, J.S. Park, B.K. Lim, S.O. Kim, J. Appl. Polym. Sci., 110, (2008), 2345-2351.
[10]. Azonano (2009), Nanocomposites [Online] http://www.azonano.com/details.sp?ArticleID=1147
[11]. O. Kamigaito, J. Jpn. Soc. Powder Powder Metall. 38 (3), (1991), 315–21.
[12]. A. de Roy, C. Forano, K. El Malki, J.P. Besse, in: Occelli M.L., Robson H.E. (Eds.), Synthesis of Microporous Materials, vol. 2, Expanded Clays and Other Microporous Systems, Van Nostrand Reinhold, New York, (1992), 108–169.
[13]. F. Trifiro, A. Vaccari, in: Atwood J.L., Davies J.E.D., MacNicol D.D., Vogtle F., Lehn J.-M., Alberti G., Bein T. (Eds.), Comprehensive Supramolecular Chemi- stry, vol. 7, Solid-State Supramolecular Chemistry: Two- and Three-Dimensional Inorganic Networks, Pergamon, Oxford, (1996), 251–291.
[14]. F. Cavani, F. Trifiro, A. Vaccari, Catal. Today 11, (1991), 173.
[15]. A.J. Marchi, C.R. Apesteguia, Appl. Clay Sci. 13, (1998), 35.
[16]. V. Rives, M. Ulibarri, Coord. Chem. Rev. 181, (1999), 61.
[17]. S. Miyata, Clays Clay Miner. 23, (1975), 369.
[18]. H.F.W. Taylor, Min. Mag. 39, (1973), 377.
[19]. C. G. Silva, Y. Bouizi, V. Fornes, H. Garcia, J. Am. Chem. Soc. , 131, (2009), 13833–13839.
[20]. V. Rives, S. Kannan, J. Mater. Chem., 10, (2000), 489–495.
[21]. R. Ma, Z. Liu, K. Takada, Iyi N., Y. Bando, T. Sasaki, J. Am. Chem. Soc., 129, (2007), 5257–5263.
[22]. Z. Liu, R. Ma, M. Osada, N. Iyi, Y. Ebina, K. Takada, T. Sasaki, J. Am. Chem. Soc., 128, (2006), 4872–4880.

[23]. H.F.W. Taylor, Miner. Mag., 37, (1973), 338.
[24]. W. Hoffmeister, H. von Platen, Cryst. Rev., 3, (1992), 3.
[25]. W. Ostwald, Studien über die Bildung und Umwandlung fester Körper. 1. Abhandlung: Übersättigung und Überkaltung. Z. Phys. Chem. 22, (1897), 289-330.
[26]. B. Li, J. He, Polym. Degrad. Stab., 83, (2004), 241.
[27]. H.L. Vandersall, Fire Flamm., 2, (1971), 97.
[28]. J.A. Rhys, Fire Mater., 4, (1980), 154.
[29]. A. Cargill, Polym. Paint Colour, 1March, (1998), 19.
[30]. R. Slysh, Paint Technol., 47, (1975), 31.
[31]. A.R. Horrocks, M.Y. Wang, M.E. Hall, F. Sunmonu, J.S. Pearson, Polym. Int., 49, (2000), 1079.
[32]. Y. Zhang, L. Q. Wang, L. J. Zou, D. F. Xue, J. Cryst. Growth, 312, (2010), 3367–3372.
[33]. J. B. Yu, Z. Jiang, L. Zhu, Z. P. Hao, Z. P. Xu, J. Phys. Chem. B, 110, (2006), 4291–4300.
[34]. K. Parida, M. Satpathy, L. Mohapatra, J. Mater. Chem., 22, (2012), 7350–7357.
[35]. R.D. Waldron, Phys. Rev. 6, (1955), 99.
001).
[36]. Li. Yuan, Powder Technology, 189, (2009), 462-465.
[37]. L. X. Jun, G. Shupping Shiyang, Spectrochim. Acta, A: Mol. Biomol. Spectrosc. 51, (1995), 519–532.
[38]. B. A. Nil, Periodico di Mineralogia, 83, (2014), 77-88.
[39]. V. Rives, Mater. Chem. Phys., 75, (2002), 19–25.
[40]. C. Jaubertie, M. J. Holgado, M. S. San Roman, V. Rives, Chem. Mater., 18, (2006), 3114–3121.
[41]. M. Vucelic, W. Jones, G. D. Moggridge, Clays Clay Miner., 45, (1997), 803–813.J. B. Yu, Z., L. Zhu, Z. P. Hao, Z. P. Xu, J. Phys. Chem. B, 110, (2006), 4291–4300.
[42]. H. E. Eltepe, Devrim Balkose, Semra Ulku, Ind. Eng. Chem. Res. 46, (2007), 2367-2371.
[43]. D. M. Schubert, US Patent No. 5,342,553 (1994).
[44]. N. P. Nies, L. Beach, R. W. Hulbert, US Patent No. 3,649,172, (1972).
[45]. H. Igarashi, A. Tatebe, K. Sakao, EP Patent No.1,205,439A1,

A. Nour El-Dein. "Fire-Resistivity personification of waterborne intumescent flame-Retardant nano-Coatings for steel structures: Synthesis and Characterization." International Journal of Engineering Research and Applications (IJERA), vol. 7, no. 8, 2017, pp. 85–94.